The FASEB Journal

FASEB
Federation of American Societies for Experimental Biology

RESEARCH ARTICLE OPEN ACCESS

Magnetic Nanoparticles Combined With Pulsed Electromagnetic Field Alleviate Chondrocyte Necroptosis in Osteoarthritis

Xuqing Li[1] | Jianhua Li[1] | Zhongyin Ji[2] | Changsheng Li[1] | Tao Wu[1] | Haixin Song[1] | Xiaotian Yang[1]

[1]Department of Rehabilitation Medicine, Sir Run Run Shaw Hospital, Zhejiang University School of Medicine, Hangzhou, China | [2]Department of Orthopaedic Surgery, Sir Run Run Shaw Hospital, Zhejiang University School of Medicine, Hangzhou, China

Correspondence: Xiaotian Yang (xiaotian.yang@zju.edu.cn)

Received: 20 August 2024 | **Revised:** 11 April 2025 | **Accepted:** 7 May 2025

Funding: This work was supported by the National Natural Science Foundation of China (No. 82102646).

Keywords: MIL-101(Fe) | necroptosis | osteoarthritis | pulsed electromagnetic field

ABSTRACT

Chondrocyte necroptosis contributes to the pathogenesis of osteoarthritis (OA). Pulsed electromagnetic field (PEMF) is a potentially useful treatment for OA. Here, magnetic nanoparticles and PEMF generate magneto-mechanical forces for regulating signaling pathways, but their effectiveness remains unclear. This study investigated whether magnetic nanoparticles (MIL-101(Fe)) combined with PEMF alleviate chondrocyte necroptosis in OA. Destabilization of the medial meniscus (DMM) surgery was performed to induce OA in 10-week-old wild-type mice. MIL-101(Fe) and PEMF were applied in human OA chondrocytes and experimental OA mice. Characterization and biocompatibility of MIL-101(Fe) were examined. Chondrocyte necroptosis was analyzed by western blotting, immunofluorescence, TUNEL, and transmission electron microscopy. OA severity was assessed by RT-PCR, immunofluorescence, histology, and micro-CT. We found that MIL-101(Fe) had no obvious cytotoxicity and presented biocompatibility. The combination of MIL-101(Fe) and PEMF ameliorated cartilage metabolism. PEMF attenuated cartilage degeneration and trabecular bone microarchitecture; these protective effects were enhanced by MIL-101(Fe). Further, the combination therapy markedly inhibited chondrocyte necroptosis and significantly decreased phosphorylation of RIP1, RIP3, and MLKL. Together, our findings indicate that MIL-101(Fe) combined with PEMF synergistically ameliorates chondrocyte necroptosis and OA progression without severe side effects, suggesting that this combination therapy may offer a novel strategy for treating OA.

1 | Introduction

Osteoarthritis (OA) is a common joint disease characterized by cartilage degeneration, subchondral bone remodeling, and synovitis [1]. Low-grade chronic inflammation has a central role in the pathogenesis of OA [2], but its pathomechanism is still poorly understood. Increasing evidence suggests that tumor necrosis factor α (TNF-α) induced chondrocyte necroptosis is

Abbreviations: ACAN, aggrecan; BV/TV, bone volume/total volume; CCK-8, cell counting kit-8; Col10a1, collagen type × alpha 1; Col2a1, collagen type ii alpha 1; DMM, destabilization of the medial meniscus; ECM, extracellular matrix; FBS, fetal bovine serum; FTIR, fourier transform infrared; HE, hematoxylin–eosin; Micro-CT, micro computed tomography; MLKL, mixed lineage kinase domain-like protein; MMP13, matrix metallopeptidase 13; MOF, metal–organic framework; OA, osteoarthritis; OARSI, Osteoarthritis Research Society International; PEMF, pulsed electromagnetic field; PXRD, powder x-ray diffractometer; RIP1, receptor-interacting protein kinase 1; RIP3, receptor-interacting protein kinase-3; ROS, reactive oxygen species; Runx2, runt-related transcription factor 2; SD, standard deviation; SEM, scanning electron microscope; SOX9, sex determining region Y-box9; Tb.N, trabecular number; Tb.Sp, trabecular separation; Tb.Th, trabecular thickness; TEM, transmission electron microscopy; TNF-α, tumor necrosis factor α; UV–Vis, ultraviolet–visible.

Xuqing Li, Jianhua Li, and Zhongyin Ji contributed equally to this work.

involved in OA pathogenesis [3–6]. Necroptosis is primarily regulated by receptor-interacting protein kinase 1 (RIP1), receptor-interacting protein kinase-3 (RIP3) and mixed lineage kinase domain-like protein (MLKL) [7]. Chondrocyte necroptosis affects cartilage degeneration and contributes to the progression of OA.

Current treatments have limited efficacy for attenuating OA progression. Pulsed electromagnetic field (PEMF), a safe and noninvasive intervention, has been proposed as a potential treatment for OA. PEMF has been shown to prevent cartilage degeneration [8] and maintain subchondral trabecular bone microarchitecture [9]. There is also some evidence to suggest that PEMF inhibits chondrocyte apoptosis and inflammation, and promotes chondrocyte autophagy and extracellular matrix production [10–12]. Further, our previous study showed that PEMF modulates chondrocyte death and attenuates the progression of OA, at least partly, through inhibiting the expression of proinflammatory cytokine TNF-α [11]. While current studies related to the mechanism of PEMF in ameliorating cartilage degeneration primarily focus on apoptosis, its impact on chondrocyte necroptosis remains unclear. Additionally, PEMF with wide spatial coverage made penetrating to specific tissues difficult, which may limit its therapeutic effectiveness. Therefore, elucidating the targeting effects and underlying mechanisms of PEMF on chondrocyte necroptosis is essential for optimizing the efficacy of PEMF therapy in OA.

Remote magnetic actuation can be targeted and precise through the combination of magnetic nanoparticles and PEMF. Vinhas et al. found that PEMF combined with iron oxide magnetic nanoparticles inhibited inflammatory mediators and matrix metalloproteinases in tendon cells under an inflammatory environment [13]. This suggests that magnetic nanoparticles may enhance the anti-inflammatory effects of PEMF. Iron-containing magnetic nanoparticles have been shown to promote bone regeneration when combined with PEMF [14]. In addition, Ji et al. suggested that the treatment targeting chondrocytes must penetrate cartilage to a certain depth, while specific nanoparticles can quickly penetrate into the deep layer of OA cartilage and remain stable [15]. MIL (Materials Institute Lavoisier) family, as a type of metal–organic framework (MOF) nanoparticles, are widely used based on their porosity, high specific surface area, biocompatibility, and biodegradability, giving them an advantage in biomedical applications compared to rigid nanoparticle carriers [16]. Fe-based MOFs exhibit a higher dielectric constant compared to Zn-based MOFs (e.g., ZIF-8). This property allows MIL-101(Fe) to efficiently convert PEMF energy into therapeutic effects. Chen et al. observed that EG@PZA effectively suppresses oxidative stress-induced extracellular matrix degradation and also ameliorates OA [17]. However, EG@PZA's Zn-based framework lacks the magnetic properties required for PEMF-enhanced targeting and energy transduction. Additionally, the Fe-based MOFs, particularly MIL-101(Fe), showed less cytotoxicity than the Zr- or Zn-based ones like UiO-66 or ZIF-8, ensuring safer long-term use in the treatment of OA [18]. Further, MIL-101(Fe) maintains structural stability in acidic conditions, which mimic the synovial fluid conditions in OA joints. MIL-101(Fe) exhibits a pH-responsive drug release property, suppressing drug release in normal chondrocytes (pH 7.4) while enhancing localized drug bioavailability in the acidic microenvironments (pH 5.0–6.5) of inflamed chondrocytes, thereby offering a potential targeted strategy for managing chronic inflammatory disorders. A previous study found that the co-delivery of HIF-2α siRNA and curcumin using MIL-101(Fe) synergistically reduced OA progression by targeting inflammation and hypoxia [19]. Therefore, we hypothesized that MIL-101(Fe) may enhance the protective effects of PEMF on chondrocyte necroptosis and OA development.

In this study, we investigated whether MIL-101(Fe) combined with PEMF alleviates chondrocyte necroptosis in OA through the RIP1/RIP3/MLKL pathway in vitro and in vivo. We also examined the effects of MIL-101(Fe) combined with PEMF on OA progression in a murine destabilization-induced model.

2 | Materials and Methods

2.1 | Animals

This study was approved by the Institutional Animal Care and Use Committee of Zhejiang University School of Medicine (ZJU20240041). Fifty 10-week-old male C57BL/6 wild-type mice were obtained from the Model Animal Research Centre of Zhejiang University School of Medicine. All mice were housed in individually ventilated cages (5 mice/cage) under pathogen-free conditions in a temperature-controlled facility (22°C ± 1°C, 12-h light/dark cycle) with ad libitum access to standard food and water.

Fifty mice were randomly divided into five groups ($n = 10$ each) respectively: sham group (sham operation with PBS injection), destabilization of the medial meniscus (DMM) group (DMM with PBS injection), DMM + PEMF group (DMM with PEMF exposure and PBS injection), DMM + MIL-101(Fe) group (DMM with MIL-101(Fe) injection), and DMM + MIL-101(Fe) + PEMF group (DMM with MIL-101(Fe) injection and PEMF exposure). An independent researcher not involved in subsequent experiments assigned codes to all mice prior to surgery. Group allocation was randomized using a computer-generated sequence (Microsoft Excel). Surgeons performed all procedures using coded animal IDs only. Evaluators were unaware of group assignments until statistical analysis was completed. The OA model was induced by the DMM surgery on the right knee joints as described previously [20]. In the sham group, the joint capsule inside the right knee joint was incised but the left medial meniscotibial ligament was intact. Four weeks after surgery, mice were intra-articular injected with 10 μL solution into the right knee joints once per week for 4 weeks; the mice in the PEMF groups were exposed to PEMF for 4 weeks. All mice were sacrificed 8 weeks post-surgery. No animals were excluded from analysis.

2.2 | Chondrocyte Isolation and Culture

Human cartilage samples were obtained from OA individuals undergoing total knee arthroplasty. The Ethics Committee of the Sir Run Run Shaw Hospital approved this research, and informed consent was obtained from all patients or their relatives prior to

TABLE 1 | The primer sequences used for RT–PCR.

Gene	Forward primer	Reverse primer
GAPDH	CTCAACTACATGGTCTACATGTTCCA	CTTCCCATTCTCAGCCTTGACT
Sox9	CAGTCCCAGCGAACGCACAT	TGCTGCTGCTGCTCGCTGTA
Col 2a1	CTTAGGACAGAGAGAGAAGG	ACTCTGGGTGGCAGAGTTTC
ACAN	TCCACATCAGAAGAGCCATAC	AGTCAAGGTCGCCAGAGG
MMP13	AAAGAACATGGTGACTTCTACC	ACTGGATTCCTTGAACGTC
Col10a1	ATATCCTGGGGATCCAGGTC	TCCAGGTTCACCTCTTGGAC
RUNX2	GAACCAAGAAGGCACAGAC	AATGCGCCCTAAATCACTG

surgery. To isolate chondrocytes, cartilage slices were digested by 30 min incubation with 0.25% trypsin followed by type II collagenase for 6 h. The harvested chondrocytes were filtered with a 70 μm cell strainer and rinsed using sterile PBS. The primary chondrocytes were cultured in DMEM/F12 with 10% fetal bovine serum (FBS) and 1% penicillin and streptomycin. To maintain phenotype integrity, we only used primary chondrocytes.

2.3 | Synthesis and Characterizations of MIL-101(Fe)

Firstly, 0.658 g (3.96 mmol) of BDC and 1.07 g (3.96 mmol) of $FeCl_3 \cdot 6H_2O$ were dissolved in 90 mL of DMF in a 250 mL round-bottomed flask. Then, 3.6 mL of acetic acid was added to the reaction mixture, which was further heated at 110°C for 24 h. After cooling to room temperature, the product was isolated by centrifugation and washed with DMF twice daily for 2 days to activate the MIL-101(Fe). The resulting brick-red solid was washed with PBS buffer solution using the same procedure to replace DMF, and subsequently soaked in PBS buffer solution for further application.

The crystalline nature of MIL-101(Fe) was analyzed using a powder X-ray diffractometer (PXRD) (D8 Advance, Bruker, Germany). The surface morphology of MIL-101(Fe) was studied using a scanning electron microscope (SEM) (Hitachi S-4800, Hitachi, Japan). Functional groups of MIL-101(Fe) were analyzed by fourier transform infrared (FTIR) spectroscopy (iS50, Thermo Fisher Scientific, Dublin, Ireland). Ultraviolet–visible (UV–Vis) spectrophotometer (UV-3600i Plus, Shimadzu Corporation, Kyoto, Japan) was used to characterize the optical absorbance of MIL-101(Fe).

2.4 | Cell Viability

The Cell Counting Kit-8 (CCK-8) assay was used to detect cell viability after treatment with the different concentrations of MIL-101(Fe). Briefly, chondrocytes were seeded into 96-well plates at a density of 1×10^4 cells/well and cultured for 24 h. Then, the cells were treated with MIL-101(Fe) at concentrations of 0, 5, 10, 20, 40, 80, and 160 μg/mL for 24 h, respectively. Further, chondrocytes were exposed to the selected concentrations of MIL-101(Fe) for 7 days. CCK8 was added to each well; the plate was then incubated at 37°C with 5% CO_2 for 2 h. The absorbance of each well was measured at 450 nm using a multi-well fluorescent plate reader (Thermo Fisher Scientific, Waltham, MA).

2.5 | PEMF Treatment

The PEMF waveform used in the experiment (duty ratio, 50%; pulse width, 6.67 ms; pulse wait, 6.67 ms) repeated at 75 Hz. The peak magnetic field intensity was 1.6 mT measured using a hand-held Gaussmeter (HT201, Hengtong, Shanghai, China). The PEMF exposure was applied for 2 h/day for 7 days in vitro and 4 weeks in vivo, respectively. Non-treated samples were placed under the same condition for the equal time with the power turned off.

2.6 | Real-Time Polymerase Chain Reaction (RT-PCR)

Total RNA isolated from chondrocyte was extracted using Trizol reagents (Invitrogen Life Technologies, Carlsbad, CA, USA) and subsequently reverse transcribed into cDNA using the PrimeScript RT reagent kit (Takara Bio, Japan). RNA quantification was performed using a CFX RT-PCR system (Bio-Rad, Hercules, CA, USA) with the SYBR Premix Ex Taq II kit (Takara Bio, Japan) according to the manufacturer's protocol. GAPDH was used as an internal reference. Target gene expression levels were normalized to GAPDH and calculated using the $2^{-\Delta\Delta Ct}$ method. The primers used in this study are shown in Table 1.

2.7 | Western Blotting

Western blotting was performed using antibodies against p-RIP1 (Cat. AP1230, 1:1000; ABclonal), RIP1 (Cat. A7414, 1:1000; ABclonal), p-RIP3 (Cat. AP1260, 1:1000; ABclonal), RIP3 (Cat. A5431, 1:1000; ABclonal), p-MLKL (Cat. AP0949, 1:1000; ABclonal), MLKL (Cat. A21894, 1:1000; ABclonal), and β-actin (Cat. AC026, 1:5000; ABclonal). Subsequently, the proteins were probed with horseradish peroxidase (HRP)-conjugated secondary antibodies and visualized using a ChemiDoc Imaging System (Bio-Rad Laboratories, Hercules, CA, United States). The relative quantity of proteins is presented as the ratio of target proteins to β-actin.

2.8 | Micro Computed Tomography (Micro-CT) Analysis

Knee joints from the mice were harvested. After surrounding muscles were removed, specimens were fixed in 4% paraformaldehyde for 48 h. Then, specimens were scanned using a micro-CT system (Skyscan 1275, Aartselaar, Belgium) with a 50 kV scanning voltage and 9 μm scan thickness. Three-dimensional reconstruction and quantitative analyses were performed using the SkyScan 3D visualization software. The tibial plateau was selected as the region of interest. The following parameters were analyzed: bone volume/total volume (BV/TV), trabecular thickness (Tb.Th), trabecular number (Tb.N), and trabecular separation (Tb.Sp).

2.9 | Histological Analysis

Joint specimens were decalcified using 20% ethylenediaminetetraacetic acid for 7 days, subjected to dehydration, embedded in paraffin, and sectioned at 5 μm slices. Tissue sections were stained with Safranin O/Fast Green for the histological assessment of cartilage. Cartilage degeneration of femoral condyle and tibial plateau was assessed according to the Osteoarthritis Research Society International (OARSI) scoring system [21]. The organ sections were stained with hematoxylin–eosin (HE); this observation was based on qualitative comparisons.

2.10 | Immunofluorescence and TUNEL Staining

Chondrocytes were seeded on 24-well plates for p-RIP1, RIP1, P-RIP3, RIP3, p-MLKL, and MLKL staining. After the treatment, chondrocytes were fixed with 4% paraformaldehyde for 25 min, washed with PBS three times, and then incubated with goat serum for 30 min. Then, cells were incubated with primary antibody (p-RIP1, RIP1, P-RIP3, RIP3, p-MLKL and MLKL) overnight at 4°C. After washing with PBS for 3 times, cells were incubated with biotinylated goat anti-rabbit secondary antibody in darkness for 1 h. The cell nuclei were stained with DAPI for 15 min. Immunofluorescence staining was also performed in cartilage specimens. Tissue sections were incubated overnight at 4°C with primary antibodies: Collagen Type II, p-RIP1, RIP1, P-RIP3, RIP3, p-MLKL, and MLKL, followed by incubation with secondary antibodies and being counterstained with DAPI. TUNEL staining was used to detect chondrocyte apoptosis. After the treatment, the chondrocytes were fixed and stained with a TUNEL Apoptosis Detection Kit (Alexa Fluor 488, Yeasen, China) according to the manufacturer's recommendations. Ultimately, images were obtained using a fluorescence microscope.

2.11 | Transmission Electron Microscopy (TEM)

Joint specimens, measuring approximately 1.5 mm^3, were immersion-fixed for 8 h in 2.5% glutaraldehyde and stored at 4°C. Subsequently, samples were fixed with 2% OsO4 for 2 h after being washed 3 times with 0.1 M phosphate-buffered saline (pH 7.4). Samples were dehydrated through increasing concentrations of ethanol. Following embedding in epoxy resin, samples were cut into 100 nm sections and were subsequently double-stained with 6% uranyl acetate and lead citrate. Images were obtained using a Tecnai G2 20 TWIN electron microscope.

2.12 | Statistical Analysis

All data were presented as mean ± standard deviation (SD). Statistical analyses were performed using GraphPad Prism version 9 (GraphPad Software, San Diego, CA, United States). To examine the differences between groups, we used one-way ANOVA followed by a Bonferroni multiple comparison test when variances were homogeneous, and Welch's ANOVA followed by a Games-Howell post hoc test when variances were heterogeneous. Assumptions were checked using the Shapiro–Wilk test for normality and Bartlett's test for homogeneity of variance. p values < 0.05 were considered statistically significant.

3 | Results

3.1 | Synthesis and Characterizations of MIL-101(Fe)

The synthesis progress of MIL-101(Fe) was shown in Figure 1A. According to the SEM images (Figure 1B), MIL-101(Fe) exhibited regular octahedron structures with an average size of around 200 nm. The PXRD pattern of MIL-101(Fe) displayed characteristic diffraction peaks, thus confirming that the synthesized MIL-101(Fe) is a single pure phase in accordance with a previous study [22] (Figure 1C). The FTIR spectra analysis showed that MIL-101(Fe) had similar characteristic peaks before and after PEMF treatment (Figure 1D). The UV–Vis absorption spectra analysis of MIL-101(Fe) was also investigated; the absorbance peak was not significantly different before and after PEMF treatment (Figure 1E).

3.2 | Biocompatibility of MIL-101(Fe)

Primary chondrocytes from OA patients received corresponding interventions (Figure 2A). To evaluate the cytotoxicity of MIL-101(Fe), the cell viabilities after incubation with varied concentrations of nanoparticles for 24 h were measured by the CCK-8 test. The chondrocyte survival rate was increased when the concentration was 10 μg/mL (Figure 2B). In this study, we finally selected 10 μg/mL as the concentration of MIL-101(Fe). MIL-101(Fe) at a concentration of 10 μg/mL showed no significant differences in cell viability compared with the control group during 7 days (Figure 2C). Further, to evaluate the in vivo biocompatibility of MIL-101(Fe), the major organs (heart, liver, spleen, lung, and kidney) of mice were evaluated by the HE staining. No noticeable abnormality was observed in these organs.

3.3 | MIL-101(Fe) Combined With PEMF Ameliorates Chondrocyte Necroptosis Through the RIP1/RIP3/MLKL Pathway

To investigate the effect of MIL-101(Fe) combined with PEMF on chondrocyte necroptosis, we first examined the expression

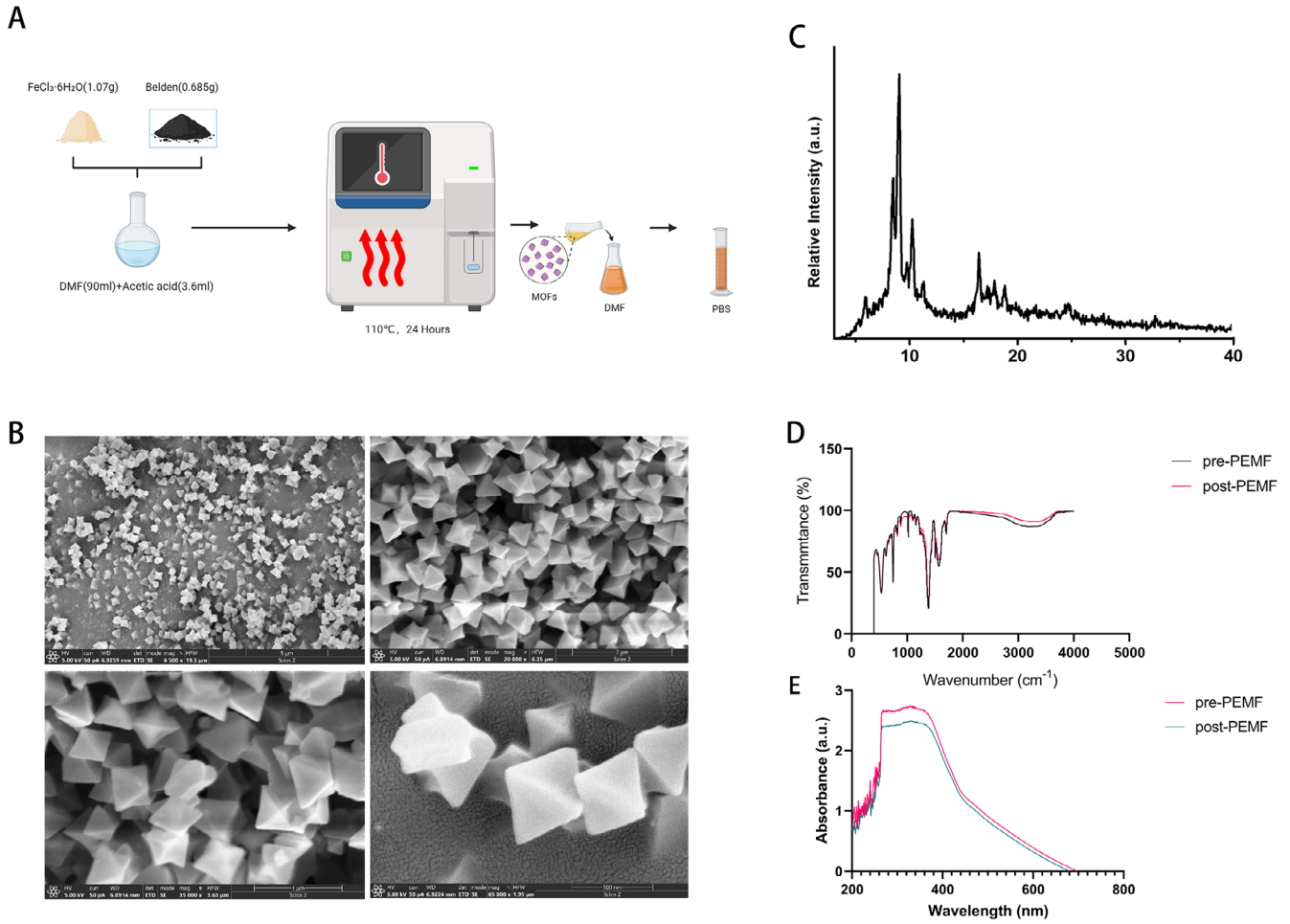

FIGURE 1 | Synthesis and characterizations of MIL-101(Fe). (A) Schematic diagram of the MIL-101(Fe) synthesis process. (B) SEM of MIL-101(Fe). (C) The PXRD pattern of MIL-101(Fe). (D) The changes of FT-IR spectra in MIL-101(Fe). (E) The UV–Vis absorption spectra analysis of MIL-101(Fe).

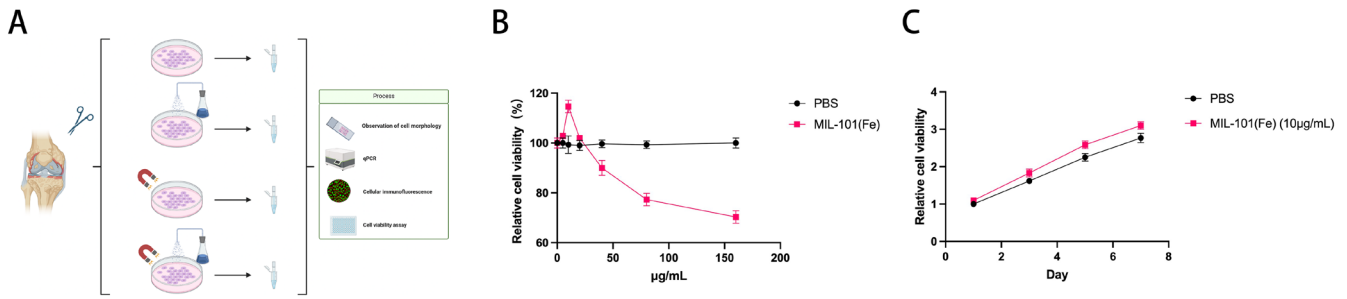

FIGURE 2 | Schematic diagram of the primary chondrocyte experiments and biocompatibility of MIL-101(Fe). (A) Schematic diagram of the primary chondrocyte experiments. (B) Effects of different concentrations of MIL-101(Fe) on cell viability for 24 h. (C) Effects of MIL-101(Fe) at a concentration of 10 μg/mL on cell viability for 7 days.

of RIP1, RIP3, and MLKL in human OA chondrocytes. Western blotting analysis showed that MIL-101(Fe) combined with PEMF did not affect the total protein expression of RIP1, RIP3, and MLKL, but significantly inhibited their phosphorylation (Figure 3A,B). We also investigated the effect of MIL-101(Fe) combined with PEMF on cartilage extracellular matrix (ECM) degradation in human OA chondrocytes, finding that PEMF and MIL-101(Fe) upregulated catabolic factors (Sex determining region Y-box9 (Sox9), aggrecan (ACAN), and collagen type II alpha 1 (Col2a1)) and downregulated anabolic factors (Runt-related transcription factor 2 (RUNX2), matrix metallopeptidase 13 (MMP13), and collagen type × alpha 1 (Col10a1)) mRNA expression in chondrocytes; these protective effects were enhanced by the combination of MIL-101(Fe) and PEMF (Figure 3C). Immunofluorescence analysis further confirmed that PEMF reduced phosphorylation of RIP1, RIP3, and MLKL in human OA chondrocytes, which was further reduced when combined with MIL-101(Fe) (Figure 3D–F). We performed the TUNEL assay to determine the degree of cell death, finding that MIL-101(Fe) combined with PEMF reduced the proportions

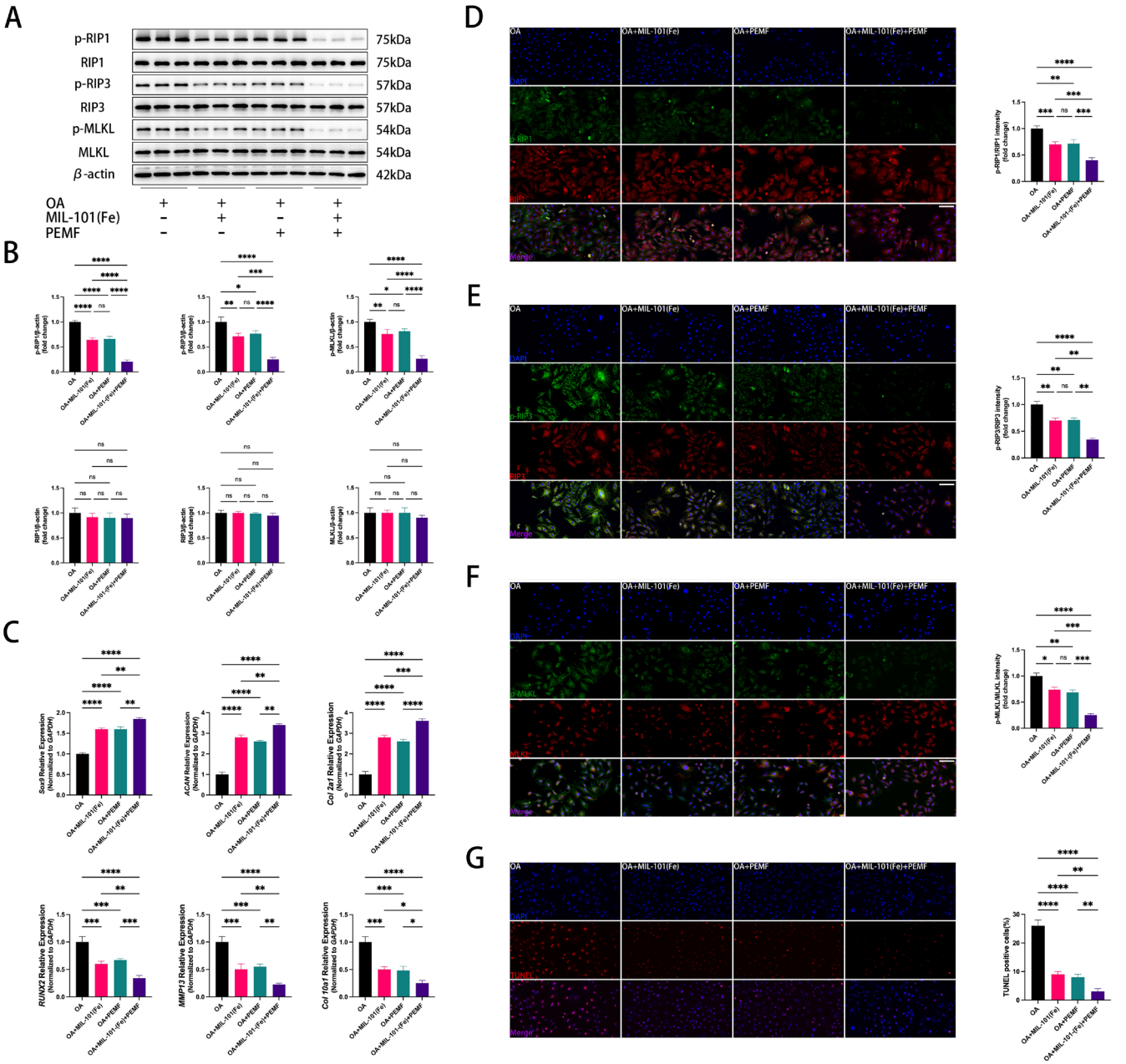

FIGURE 3 | MIL-101(Fe) combined with PEMF ameliorates chondrocyte necroptosis through the RIP1/RIP3/MLKL pathway in human primary chondrocytes (A, B) p-RIP1, RIP1, p-RIP3, RIP3, p-MLKL, and MLKL protein expression revealed by Western blotting. $n = 5$. (C) RT-PCR analysis of Sox9, ACAN, Col 2a1, RUNX2, MMP13, and Col10a1. $n = 5$. (D–F) Representative images and quantification of immunofluorescence staining of p-RIP1, RIP1, p-RIP3, RIP3, p-MLKL, and MLKL (Scalebar = 30 μm). $n = 5$. (G) Representative images and quantification of immunofluorescence staining of TUNEL in human primary chondrocytes (Scalebar = 30 μm). $n = 5$. *$p < 0.05$, **$p < 0.01$, ***$p < 0.001$, ****$p < 0.0001$, ns, no statistical significance. The data are presented as the mean ± SD.

of TUNEL positive cells compared to the other groups in vitro (Figure 3G).

In DMM mice, immunofluorescence analysis also confirmed that MIL-101(Fe) combined with PEMF reduced phosphorylation of RIP1, RIP3, and MLKL (Figure 4A–C). To discern normal and necrotic chondrocytes in more detail, we performed TEM to observe the cellular ultrastructural changes. Chondrocytes exhibited intact organelles and cell membranes in the sham group. In OA chondrocytes, swollen organelles and ruptured cell membranes were frequently found, presenting low electron density. Compared to the DMM group, the PEMF group exhibited a significantly lower proportion of necrotic chondrocytes, which was further reduced when combined with MIL-101(Fe) (Figure 4D).

3.4 | MIL-101(Fe) Combined With PEMF Alleviates OA Development

Consistent with our findings in chondrocytes, immunofluorescence results showed that the decreased expression of Col2a in articular cartilage after DMM surgery was upregulated after treatment with PEMF, MIL-101(Fe) and combination therapy, respectively (Figure 5A,B). Moreover, MIL-101(Fe) combined with

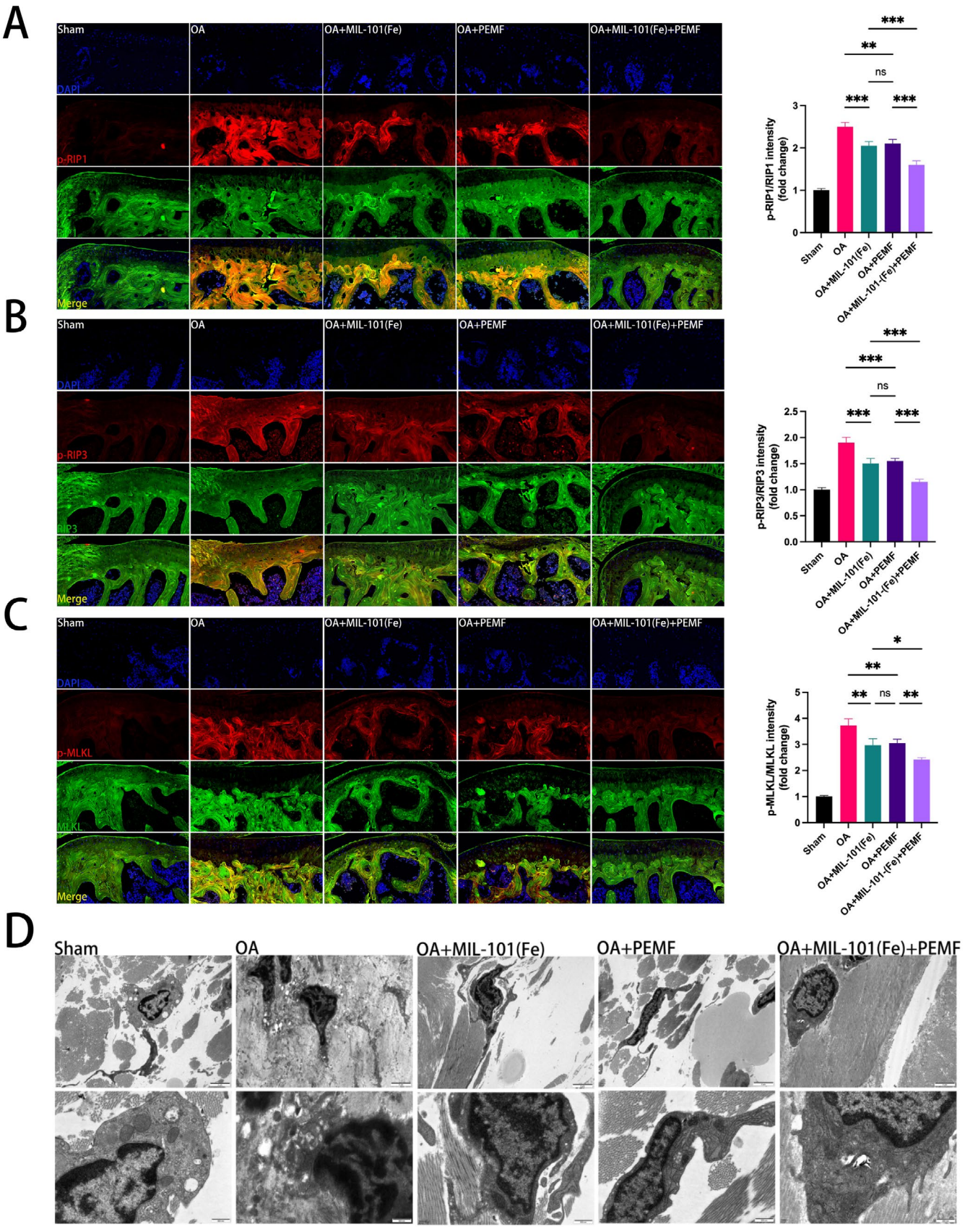

FIGURE 4 | MIL-101(Fe) combined with PEMF ameliorates chondrocyte necroptosis through the RIP1/RIP3/MLKL pathway in mice (A–C) Representative images and quantification of immunofluorescence staining of p-RIP1, RIP1, p-RIP3, RIP3, p-MLKL, and MLKL in the knee joints of mice. $n = 5$. (D) TEM of chondrocytes in joints from mice. (Scalebar = 2 μm, 500 nm). $n = 3$. *$p < 0.05$, **$p < 0.01$, ***$p < 0.001$, ns, no statistical significance. The data are presented as the mean ± SD.

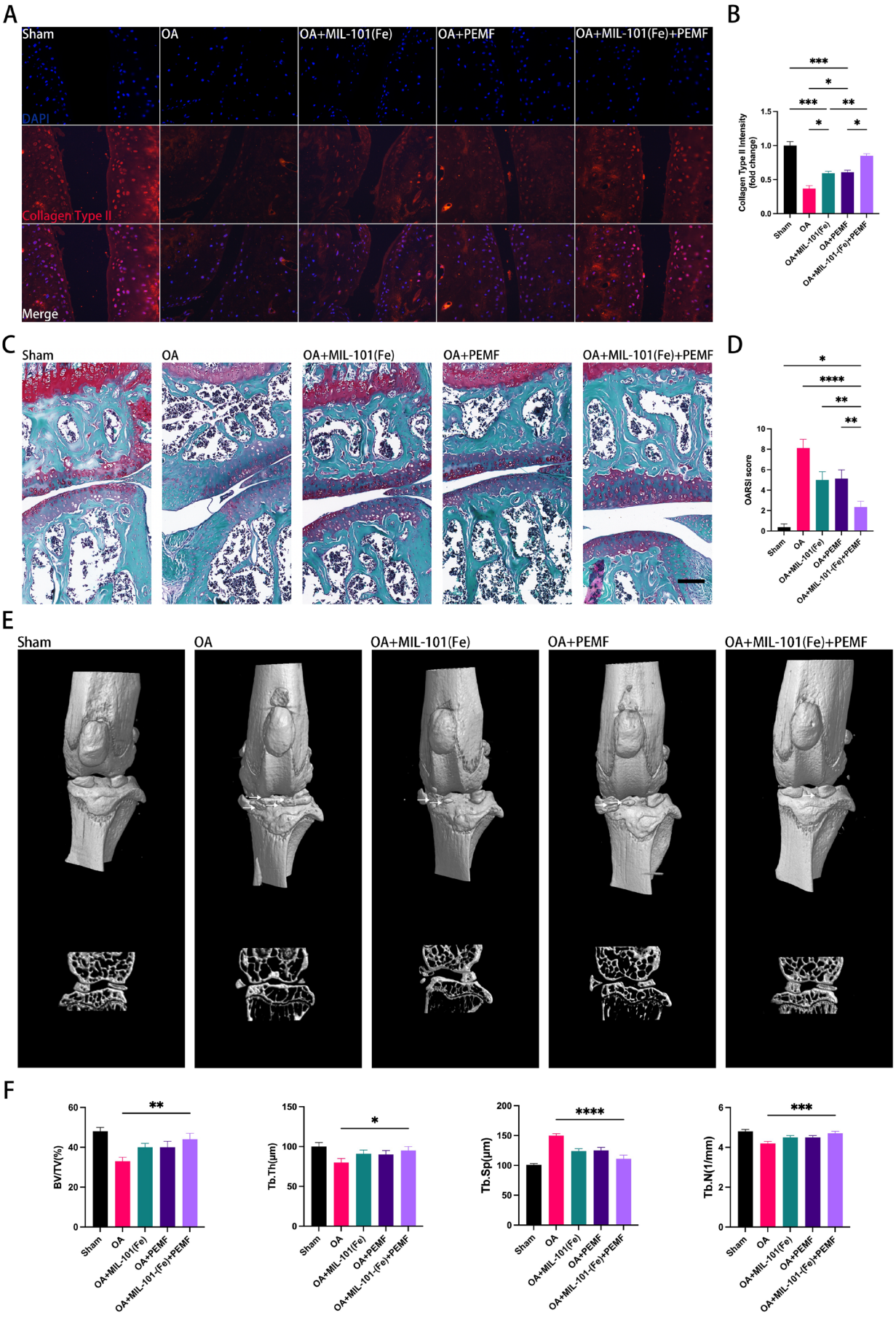

FIGURE 5 | Legend on next page.

FIGURE 5 | MIL-101(Fe) combined with PEMF alleviates OA development in mice. (A, B) Representative images and quantification of immunofluorescence staining of Collagen Type II in the knee joints of mice. $n = 5$. (C) Representative images of Safranin O/fast green staining. (D) OARSI score. (E) Representative micro-CT 3D and cross-sectional images of the knee joints of mice. (F) Bone volume/total volume (BV/TV), trabecular thickness (Tb.Th), trabecular separation (Tb.Sp), and trabecular number (Tb.N). $n = 5$. $^{*}p < 0.05$, $^{**}p < 0.01$, $^{***}p < 0.001$, $^{****}p < 0.0001$, ns, no statistical significance. The data are presented as the mean ± SD.

PEMF exhibited less cartilage erosion and proteoglycan loss in the articular cartilage compared to the DMM group, which was further validated by OARSI score analysis (Figure 5C,D). To further assess the effect of combination therapy on subchondral bone changes, we examined the trabecular bone microarchitecture by micro-CT analysis; MIL-101(Fe) combined with PEMF significantly increased BV/TV, Tb.Th, and Tb.N, and decreased Tb.Sp compared to the DMM group (Figure 5E,F). Together, these results suggest that MIL-101(Fe) combined with PEMF alleviates OA development.

4 | Discussion

Our study suggests that MIL-101(Fe) combined with PEMF ameliorates chondrocyte necroptosis by inhibiting the RIP1/RIP3/MLKL pathway in human OA chondrocytes and a murine destabilization-induced OA model. Further, MIL-101(Fe) combined with PEMF has a beneficial effect on cartilage degeneration and trabecular bone microarchitecture. These findings demonstrate that MIL-101(Fe) combined with PEMF alleviates OA progression; the combination therapy shows larger intervention effects than the use of MIL-101(Fe) or PEMF alone.

In our study, MIL-101(Fe) showed no obvious cytotoxicity and presented high biocompatibility. Our findings suggest that MIL-101(Fe) may be a safe and promising strategy in the treatment of OA. Similarly, Zhang et al. observed that MIL-101-NH2 had no obvious cytotoxicity against chondrocytes even at high concentrations (400 μg/mL) and the induced reactive oxygen species (ROS) level was negligible [19]. MIL-101(Fe) has been utilized in many areas, including bioimaging, drug delivery, antibacterial, biosensing [23–26], while the functionalization of organic linkers can bring unique properties and expand the variety of magnetic nanoparticles. Further investigation is required to understand how functional groups influence magnetic nanoparticles.

The responsive magnetic nanoparticles and magnetic field are the two primary components of magnetic actuation, which could activate mechanotransduction signaling pathways through the application of magnetic force. The utilization of magnetic nanoparticles enables the condensing of PEMF energy in nanoscale volumes by several orders of magnitude. PEMF may help in the accumulation of magnetic nanoparticles at a desired site. The effects can be localized at the molecular or cellular level. Using magnetic nanoparticles in conjunction with PEMF can provide higher degrees of control over signaling pathways and mechanosensors [27, 28].

For the in vivo mouse model, we previously observed that daily 1-h PEMF exposure over 4 weeks attenuates OA progression in the DMM model [11]. To enhance therapeutic efficacy while maintaining translational relevance, we extended the daily PEMF exposure to 2 h, a regimen supported by studies in larger animal models (e.g., Guinea pigs) showing improved outcomes with prolonged daily treatment (6 h/day) [29]. This adjustment aimed to balance efficacy and practicality, as excessively long daily treatments in mice may complicate clinical translation. In vitro, Vincenzi et al. [30] demonstrated enhanced anti-inflammatory effects in human chondrocytes after a single 24-h PEMF exposure, while another study by Anbarasan et al. [31] applied PEMF for 1 h/day over 3 days to modulate chondrocyte extracellular matrix metabolism. These differences highlight the "window effect" of PEMF, where outcomes depend critically on specific parameters. Extending treatment beyond this period in monolayer cultures risks confounding outcomes due to dedifferentiation or senescence. The 7-day in vitro duration is consistent with recent findings demonstrating that PEMF-induced chondrogenic differentiation of bone marrow mesenchymal stem cells (BMSCs) peaks within this timeframe. Importantly, extending PEMF exposure to 14 days diminished these pro-chondrogenic effects, suggesting a therapeutic efficacy window within the first week in vitro [32].

Our data showed a beneficial effect of MIL-101(Fe) combined with PEMF on chondrocyte necroptosis by inhibiting the expression of p-RIP1, p-RIP3, and p-MLKL, indicating that MIL-101(Fe) may enhance the protective effects of PEMF on chondrocyte death in OA. Our results are in keeping with the findings of a previous study, which found that PEMF (15 Hz, 2 mT) inhibited necroptosis of condylar chondrocytes in temporomandibular joint OA [33]. They only detected the protein expression of p-MLKL in OA rats, whereas we assessed RIP1/RIP3/MLKL-mediated necroptosis in human OA chondrocytes and OA mice. To our knowledge, we are the first to examine the effects of magnetic nanoparticles combined with PEMF in the treatment of OA. In contrast to our findings, Barati et al. found that electromagnetic field (1 Hz, 100 mT) induced necroptosis in mice with tumor [34]. Here, they used magnetic field with high intensity, whereas in our study, we used PEMF (75 Hz, 1.6 mT) with low intensity. PEMF therapy has a window effect, where different PEMF parameters have different therapeutic effects, sometimes even contradictory. Currently, the parameters of 75 Hz frequency and 1.6 mT intensity are by far the most widely studied for OA treatment.

In our study, MIL-101(Fe) combined with PEMF showed a beneficial effect on cartilage degeneration and subchondral bone remodeling, and promoted the synthesis of cartilage matrix; we observed that the beneficial effects of combination therapy were larger than MIL-101(Fe) or PEMF alone. Our findings suggest that MIL-101(Fe) combined with PEMF synergistically alleviates OA progression. More recently, Habib et al. reported that magnetic nanoparticles combined with PEMF synergistically stimulated osteogenesis in human bone marrow-derived mesenchymal stem cells [14]. We further assessed the subchondral bone microarchitecture changes in OA mice. The combined treatment of MIL-101(Fe) and PEMF has been observed to reduce bone loss in the subchondral bone during the progression of

OA. One explanation for this effect may be due to the influence on osteoclast differentiation in the subchondral bone. Previous studies suggested that PEMF could suppress osteoclastic differentiation by modulating the RANKL/RANK/OPG and Ca(2+)-calcineurin-NFATc1 signaling pathways [35, 36]. Iron oxide nanoparticles can inhibit osteoclast differentiation through the suppression of MAPK and NF-κB signaling pathways, and it combined with magnetic field may impact bone remodeling by restoring the balance between osteoblasts and osteoclasts [37]. The precise mechanisms are not yet fully understood, whereas magnetic nanoparticles and magnetic fields were able to provide magneto-mechanical stimulations for bone formation [38]. It was suggested that the magnetic properties of MIL-101(Fe) could enhance the delivery and retention of the PEMF treatment in the subchondral bone. Our results considered together suggest an association between chondrocyte necroptosis and OA progression; the synergistic therapy alleviates OA progression by inhibiting RIP1/RIP3/MLKL-mediated necroptosis.

There are several potential limitations in our study. Firstly, we only applied one concentration of MIL-101(Fe) (10 μg/mL). The concentration was given according to our cell viability results. The dose–and time-dependent responses of magnetic nanoparticles in vitro and in vivo were not investigated. Future studies should systematically explore dose–and time-dependent responses to optimize therapeutic parameters. Secondly, our results lack data on the depth of penetration and biodistribution of MIL-101(Fe) after injection. Thirdly, there is evidence to suggest that lesions are more apparent on the medial side of the joint [20], whereas in our study we did not distinguish the medial and lateral sides, which may have limited our ability to detect differences. Future studies are required to refine the regions of interest in the assessment of cartilage and subchondral bone. Further, we did not conduct in-depth research on the mechanisms by which MIL-101(Fe) combined with PEMF improves chondrocyte necroptosis; the specific molecular mechanisms by which MIL-101(Fe) enhances the effects of PEMF are still not clear. However, this study primarily focused on establishing the therapeutic efficacy and biosafety profile of MIL-101(Fe) combined with PEMF therapy. Our work provides the first conclusive evidence that magnetomechanical stimulation can modulate chondrocyte necroptosis in OA. Future investigations should use gene knockout models or inhibitors to confirm the exact role of these signals.

In summary, we observed that MIL-101(Fe) combined with PEMF alleviated chondrocyte necroptosis by inhibiting the RIP1/RIP3/MLKL pathway in OA. Our data suggest that MIL-101(Fe) may enhance the protective effects of PEMF on attenuating OA progression. We also confirmed the high biocompatibility of MIL-101(Fe) in the treatment of OA. Magnetic nanoparticles combined with PEMF may offer a novel strategy for treating OA. Further studies are required to confirm whether functionalized magnetic nanoparticles can target articular cartilage through specific mechanisms.

Author Contributions

Conception and design, X.Y. Analysis and interpretation of the data, X.L. and J.L. Drafting of the article, X.Y. and X.L. Critical revisions, T.W., H.S., and X.Y. Technical support, C.L. and Z.J. Collection of data, X.L., J.L., Z.J., and C.L. Final approval, X.L. and X.Y. All authors read and approved the final manuscript.

Acknowledgments

We would like to thank Dr. Wei Wei and Prof. Shibo Cai for making the custom-designed PEMF exposure system. We would like to thank Prof. Xueqian Kong, Prof. Zhijie Chen, and Dr. Dongdong Ma for their technical assistance.

Conflicts of Interest

The authors declare no conflicts of interest.

Data Availability Statement

The data that support the findings of this study are available from the corresponding author upon reasonable request.

References

1. D. J. Hunter and S. Bierma-Zeinstra, "Osteoarthritis," *Lancet (London, England)* 393 (2019): 1745–1759.

2. W. H. Robinson, C. M. Lepus, Q. Wang, et al., "Low-Grade Inflammation as a Key Mediator of the Pathogenesis of Osteoarthritis," *Nature Reviews Rheumatology* 12 (2016): 580–592.

3. J. Cheng, X. Duan, X. Fu, et al., "RIP1 Perturbation Induces Chondrocyte Necroptosis and Promotes Osteoarthritis Pathogenesis via Targeting BMP7," *Frontiers in Cell and Development Biology* 9 (2021): 638382.

4. J. Jeon, H. J. Noh, H. Lee, et al., "TRIM24-RIP3 Axis Perturbation Accelerates Osteoarthritis Pathogenesis," *Annals of the Rheumatic Diseases* 79 (2020): 1635–1643.

5. S. W. Lee, J. H. Rho, S. Y. Lee, et al., "Leptin Protects Rat Articular Chondrocytes From Cytotoxicity Induced by TNF-α in the Presence of Cyclohexamide," *Osteoarthritis and Cartilage* 23 (2015): 2269–2278.

6. Y. Gong, J. Qiu, J. Ye, et al., "AZ-628 Delays Osteoarthritis Progression via Inhibiting the TNF-α-Induced Chondrocyte Necroptosis and Regulating Osteoclast Formation," *International Immunopharmacology* 111 (2022): 109085.

7. Y. Dondelinger, P. Hulpiau, Y. Saeys, M. J. M. Bertrand, and P. Vandenabeele, "An Evolutionary Perspective on the Necroptotic Pathway," *Trends in Cell Biology* 26 (2016): 721–732.

8. J. Zhou, Y. Liao, H. Xie, et al., "Pulsed Electromagnetic Field Ameliorates Cartilage Degeneration by Inhibiting Mitogen-Activated Protein Kinases in a Rat Model of Osteoarthritis," *Physical Therapy in Sport* 24 (2017): 32–38.

9. X. Yang, H. He, Y. Zhou, et al., "Pulsed Electromagnetic Field at Different Stages of Knee Osteoarthritis in Rats Induced by Low-Dose Monosodium Iodoacetate: Effect on Subchondral Trabecular Bone Microarchitecture and Cartilage Degradation," *Bioelectromagnetics* 38 (2017): 227–238.

10. H. Guo, Q. Luo, J. Zhang, H. Lin, L. Xia, and C. He, "Comparing Different Physical Factors on Serum TNF-Alpha Levels, Chondrocyte Apoptosis, Caspase-3 and Caspase-8 Expression in Osteoarthritis of the Knee in Rabbits," *Joint, Bone, Spine: Revue du Rhumatisme* 78 (2011): 604–610.

11. X. Yang, H. Guo, W. Ye, L. Yang, and C. He, "Pulsed Electromagnetic Field Attenuates Osteoarthritis Progression in a Murine Destabilization-Induced Model Through Inhibition of TNF-α and IL-6 Signaling," *Cartilage* 13 (2021): 1665s–1675s.

12. J. Liu, X. Huang, J. Zhou, et al., "Pulsed Electromagnetic Field Alleviates Synovitis and Inhibits the NLRP3/Caspase-1/GSDMD Signaling

Pathway in Osteoarthritis Rats," *Electromagnetic Biology and Medicine* 41 (2022): 101–107.

13. A. Vinhas, M. T. Rodrigues, A. I. Gonçalves, R. L. Reis, and M. E. Gomes, "Magnetic Responsive Materials Modulate the Inflammatory Profile of IL-1β Conditioned Tendon Cells," *Acta Biomaterialia* 117 (2020): 235–245.

14. M. Habib, D. A. Horne, K. Hussein, et al., "Magnetic Nanoparticles Synergize With Pulsed Magnetic Fields to Stimulate Osteogenesis In Vitro," *Tissue Engineering Parts A* 27 (2021): 402–412.

15. M. L. Ji, H. Jiang, F. Wu, et al., "Precise Targeting of miR-141/200c Cluster in Chondrocytes Attenuates Osteoarthritis Development," *Annals of the Rheumatic Diseases* 80, no. 3 (2021): 356–366.

16. Z. Lin, D. Liao, C. Jiang, et al., "Current Status and Prospects of MIL-Based MOF Materials for Biomedicine Applications," *RSC Medicinal Chemistry* 14 (2023): 1914–1933.

17. Y. Chen, Y. Zhang, C. Wu, et al., "High-Throughput Screening Strategy and Metal-Organic Framework-Based Multifunctional Controlled-Release Nanomaterial for Osteoarthritis Therapy," *ACS Nano* 19 (2025): 4802–4819.

18. R. Ettlinger, U. Lächelt, R. Gref, et al., "Toxicity of Metal-Organic Framework Nanoparticles: From Essential Analyses to Potential Applications," *Chemical Society Reviews* 51 (2022): 464–484.

19. Z. J. Zhang, Y. K. Hou, M. W. Chen, et al., "A pH-Responsive Metal-Organic Framework for the Co-Delivery of HIF-2α siRNA and Curcumin for Enhanced Therapy of Osteoarthritis," *Journal of Nanobiotechnology* 21 (2023): 18.

20. S. S. Glasson, T. J. Blanchet, and E. A. Morris, "The Surgical Destabilization of the Medial Meniscus (DMM) Model of Osteoarthritis in the 129/SvEv Mouse," *Osteoarthritis and Cartilage* 15 (2007): 1061–1069.

21. S. S. Glasson, M. G. Chambers, W. B. Van Den Berg, and C. B. Little, "The OARSI Histopathology Initiative - Recommendations for Histological Assessments of Osteoarthritis in the Mouse," *Osteoarthritis and Cartilage* 18, no. Suppl 3 (2010): S17–S23.

22. Z. Dong, Y. Sun, J. Chu, X. Zhang, and H. Deng, "Multivariate Metal-Organic Frameworks for Dialing-In the Binding and Programming the Release of Drug Molecules," *Journal of the American Chemical Society* 139 (2017): 14209–14216.

23. M. Al Haydar, H. R. Abid, B. Sunderland, and S. Wang, "Metal Organic Frameworks as a Drug Delivery System for Flurbiprofen," *Drug Design, Development and Therapy* 11 (2017): 2685–2695.

24. X. Jiang, Z. Wang, H. Wang, Y. Zhuo, R. Yuan, and Y. Chai, "A Novel Metal-Organic Framework Loaded With Abundant N-(Aminobutyl)-N-(Ethylisoluminol) as a High-Efficiency Electrochemiluminescence Indicator for Sensitive Detection of mucin1 on Cancer Cells," *Chemical Communications (Cambridge, England)* 53 (2017): 9705–9708.

25. G. Wyszogrodzka, P. Dorożyński, B. Gil, et al., "Iron-Based Metal-Organic Frameworks as a Theranostic Carrier for Local Tuberculosis Therapy," *Pharmaceutical Research* 35 (2018): 144.

26. X. Ma, X. Ren, X. Guo, et al., "Multifunctional Iron-Based Metal-Organic Framework as Biodegradable Nanozyme for Microwave Enhancing Dynamic Therapy," *Biomaterials* 214 (2019): 119223.

27. L. J. Santos, R. L. Reis, and M. E. Gomes, "Harnessing Magnetic-Mechano Actuation in Regenerative Medicine and Tissue Engineering," *Trends in Biotechnology* 33 (2015): 471–479.

28. R. Sensenig, Y. Sapir, C. MacDonald, S. Cohen, and B. Polyak, "Magnetic Nanoparticle-Based Approaches to Locally Target Therapy and Enhance Tissue Regeneration In Vivo," *Nanomedicine (London, England)* 7 (2012): 1425–1442.

29. F. Veronesi, P. Torricelli, G. Giavaresi, et al., "In Vivo Effect of Two Different Pulsed Electromagnetic Field Frequencies on Osteoarthritis," *Journal of Orthopaedic Research* 32 (2014): 677–685.

30. F. Vincenzi, M. Targa, C. Corciulo, et al., "Pulsed Electromagnetic Fields Increased the Anti-Inflammatory Effect of A_2A and A_3 Adenosine Receptors in Human T/C-28a2 Chondrocytes and hFOB 1.19 Osteoblasts," *PLoS One* 8 (2013): e65561.

31. S. Anbarasan, U. Baraneedharan, S. F. Paul, H. Kaur, S. Rangaswami, and E. Bhaskar, "Low Dose Short Duration Pulsed Electromagnetic Field Effects on Cultured Human Chondrocytes: An Experimental Study," *Indian Journal of Orthopaedics* 50, no. 1 (2016): 87–93.

32. K. Song, J. Hu, M. Yang, et al., "Pulsed Electromagnetic Fields Potentiate Bone Marrow Mesenchymal Stem Cell Chondrogenesis by Regulating the Wnt/β-Catenin Signaling Pathway," *Journal of Translational Medicine* 22 (2024): 741.

33. Y. Ma, F. He, X. Chen, et al., "Low-Frequency Pulsed Electromagnetic Fields Alleviate the Condylar Cartilage Degeneration and Synovitis at the Early Stage of Temporomandibular Joint Osteoarthritis," *Journal of Oral Rehabilitation* 51 (2024): 666–676.

34. M. Barati, M. A. Javidi, B. Darvishi, et al., "Necroptosis Triggered by ROS Accumulation and ca(2+) Overload, Partly Explains the Inflammatory Responses and Anti-Cancer Effects Associated With 1Hz, 100 mT ELF-MF In Vivo," *Free Radical Biology & Medicine* 169 (2021): 84–98.

35. J. Zhang, H. Xu, Z. Han, et al., "Pulsed Electromagnetic Field Inhibits RANKL-Dependent Osteoclastic Differentiation in RAW264.7 Cells Through the ca(2+)-Calcineurin-NFATc1 Signaling Pathway," *Biochemistry and Biophysics Research Communications* 482, no. 2 (2017): 289–295.

36. J. He, Y. Zhang, J. Chen, S. Zheng, H. Huang, and X. Dong, "Effects of Pulsed Electromagnetic Fields on the Expression of NFATc1 and CAII in Mouse Osteoclast-Like Cells," *Aging Clinical and Experimental Research* 27 (2015): 13–19.

37. J. Yang, J. Wu, Z. Guo, G. Zhang, and H. Zhang, "Iron Oxide Nanoparticles Combined With Static Magnetic Fields in Bone Remodeling," *Cells* 11 (2022): 3298.

38. Y. Xia, J. Sun, L. Zhao, et al., "Magnetic Field and Nano-Scaffolds With Stem Cells to Enhance Bone Regeneration," *Biomaterials* 183 (2018): 151–170.

Supporting Information

Additional supporting information can be found online in the Supporting Information section.